Available online at www.sciencedirect.com
SCIENCE DIRECT
Journal of Colloid and Interface Science 301 (2006) 145–154
JOURNAL OF Colloid and Interface Science
www.elsevier.com/locate/jcis

Synthesis and characterization of Au core–Au–Ag shell nanoparticles from gold seeds: Impacts of glycine concentration and pH

Yu-Fen Huang, Kuan-Ming Huang, Huan-Tsung Chang *

Department of Chemistry, National Taiwan University, 1, Section 4, Roosevelt Road, Taipei, Taiwan

Received 7 January 2006; accepted 30 April 2006

Available online 5 May 2006

Abstract

This paper describes the preparation of Au core–Au–Ag shell nanoparticles (NPs) in different morphologies by controlling both the pH and the glycine concentration. Using a seed-growth method, we prepared high-quality Au core–Au–Ag shell NPs from a glycine solution under alkaline conditions (pH > 8.5). By controlling both the pH and the glycine concentration, we prepared dumbbell-shaped and peanut-shaped Au core–Au–Ag shell NPs readily by depositing gold and silver, reduced by ascorbate, onto the gold nanorods. We have found that the glycine concentration that is optimal for preparing high-quality Au core–Au–Ag shell NPs differs at the various values of pH. At pH < 8.5, the glycine concentration is not important, but, when preparing dumbbell- and peanut-shaped Au core–Au–Ag shell NPs, it should be greater than 50 mM and greater than 20 mM at pH 9.5 and 10.5, respectively. Glycine plays a number of roles during the synthesis of the Au core–Au–Ag shell NPs by controlling the solution pH, altering the reduction potentials of gold and silver ions through forming complexes with metal ions (Au^+ and Ag^+), minimizing the formation of Ag_2O, AgCl, and AgBr precipitates, and stabilizing the thus-prepared NPs. At pH 9.7, we observed the changes in the morphologies of the Au core–Au–Ag shell NPs—from regular (rectangular) to peanut- and dumbbell-shaped, and finally to jewel-, diamond-, and/or sphere-shaped—that occurred during the course of a 60-min reaction. In addition, we were able to affect the shapes and sizes of the Au core–Au–Ag shell NPs by controlling the reaction time.

Keywords: Gold nanorod; Au core–Au–Ag shell nanoparticles; Glycine

1. Introduction

There is a great deal of interest currently in the synthesis of anisotropic inorganic nanomaterials, especially nanorods (NRs) and nanowires, for their potential applications in, for instance, information technology, optoelectrics, and sensing [1–8]. For example, noble metals, such as gold, that have aspect ratios (length-to-width ratios) greater than 1, exhibit strong transverse and longitudinal surface plasmon bands in the visible region, which makes them promising agents for sensing and imaging purposes [9,10]. Because of the strong effects that size and shape have on optical properties [11–13], the preparation of nanomaterials in a variety of different morphologies remains an important and challenging task.

A number of techniques, including chemical, electrical, and optical processes, have been employed for the preparation of monodisperse samples of NRs and nanowires [14–26]. Syntheses through simple wet-chemical methods are particularly favored for the cost-effective and large-scale production of such nanostructures. These methods generally use soft and rigid templates to prepare rod-shaped metal nanoparticles [18–22]. In aqueous media, detergents such as hexadecyltrimethylammonium bromide (CTAB) may be used for the successful syntheses of gold and silver NRs [23–26]. Nikoobakht and El-Sayed used surfactant-stabilized Au seeds and different amounts of silver nitrate to prepare very high yields of gold NRs (GNRs) having various aspect ratios [25]. The growth of GNRs is believed to be governed in these cases by the preferential adsorption of CTAB to the different crystal faces during the growth process [25,27]. Thus surfactants having chains of different lengths [28], additives such as cyclohexane [29], and silver ions [25] that can assist the template elongation with its ability to induce mono-

* Corresponding author. Fax: +886 2 33661171.
E-mail address: changht@ntu.edu.tw (H.-T. Chang).

0021-9797/$ – see front matter
doi:10.1016/j.jcis.2006.04.079

layer formation, strongly influence the process of GNR formation. On the basis of those studies, it has been suggested that the properties of the surfactants and the organic solvents, the relative amounts of $NaAuCl_4$ and $AgNO_3$ with respect to the concentration of the reducing agents, and the concentration of the seeds are all important parameters for controlling the aspect ratios of GNRs when using the seed-mediated growth method.

In addition to controlling the aspect ratio, the preparation of multimetallic NRs is also of interest to both basic and applied science because they exhibit characteristic electronic, optical, and catalytic properties that differ from those of their individual constituent metals [18,30]. It is known that the longitudinal surface plasmon resonance (SPR) extinction of GNRs is enhanced and undergoes a blue shift upon coating with silver, mainly because of the changes in the dielectric function and overall aspect ratio, as well as the formation of an Au–Ag interface [30,31]. Regular rod-shaped Au–Ag core–shell nanostructures have been obtained when using NH_2OH to deposit reduced silver onto the surface of the GNRs in the absence of CTAB [31]. In the presence of such a mild reducing agent, silver ions can be reduced only at the metallic surface, but neither silver NRs nor silver nanodots are formed in the absence of GNRs. Au–Ag core–shell NRs that have different shell thicknesses can be synthesized also by chemically depositing silver onto the surface of poly(vinylpyrrolidone) (PVP)-stabilized GNRs when using ascorbic acid as a reducing agent under alkaline conditions [32]. With their much sharper and stronger, longitudinal SPR bands, relative to those of GNRs, multimetallic NRs have greater applicability for sensing biomolecules of interest.

Recently, we reported a simple procedure for the synthesis of Au–Ag nanoparticles (NPs) under alkaline conditions (pH 8.0–10.0) from silver and ascorbate ions using GNRs as seeds [30]. The silver ions that are reduced by the ascorbate ions deposit onto the surfaces of the GNRs to form dumbbell-shaped Au–Ag NPs whose morphologies differ depending on the pH and the concentration of silver ions. The formation of Au–Ag NPs suggests that the {111} facet of the GNRs is more accessible to silver atoms than is the {110} facet, upon which densely packed CTAB assemblies form [25,30]. By controlling the pH, we are able to prepare high-quality (>90%) Au–Ag NPs. We have also learned that glycine plays some important roles during the preparation of the Au–Ag NPs. For example, AgCl and AgBr do not precipitate in the presence of high concentrations of glycine, mainly because of the formation of Ag–glycine complexes. In addition, we have found that the as-prepared Au–Ag NPs are stable for over 3 months in glycine solution after the removal of CTAB, which suggests that glycine acts as a capping agent to stabilize the Au–Ag NPs. However, the role that glycine plays during the synthesis of the Au–Ag NPs and the mechanism of their formation remain unclear.

Our goal in this study was to obtain some insight into the mechanism of formation of Au core–Au–Ag shell NPs possessing different morphologies by controlling the pH and the glycine concentration—at constant concentrations of $NaAuCl_4$, $AgNO_3$, ascorbic acid, and CTAB—under alkaline conditions when using GNRs as seeds [30]. We have found that the presence of both $NaAuCl_4$ and $AgNO_3$ in the solution is necessary for the formation of the differently shaped and sized Au core–Au–Ag shell NPs. In this paper, we emphasize the effects that the glycine concentration, pH, and reaction time have on the synthesis of the differently shaped and sized Au core–Au–Ag shell NPs.

2. Experimental

2.1. Chemicals

Glycine, L-ascorbic acid (99%), silver nitrate ($AgNO_3$, 99%), and sodium tetrachloroaurate(III) dihydrate ($NaAuCl_4 \cdot 2H_2O$, 99%) were obtained from Sigma (St. Louis, MO, USA). CTAB (98%) was purchased from Acros (New Jersey, USA). Sodium borohydride ($NaBH_4$, 98%) was purchased from Aldrich (Milwaukee, WI, USA). The values of pH of the glycine solutions, which ranged from 8.5 to 10.5, were adjusted with NaOH. Deionized water (18 MΩ cm) was used to prepare all of the aqueous solutions.

2.2. Synthesis of GNR seeds

The GNR seeds were prepared using a slight modification of a seeding method described previously in Ref. [25]. CTAB solution (0.2 M, 5.0 ml) was mixed with 0.5 mM $NaAuCl_4$ (5.0 ml). Ice-cold 0.01 M $NaBH_4$ (0.6 ml) was added to this solution under sonication. Reaction of this mixture for 3 min resulted in the formation of a brownish-yellow seed solution. In the growth solution, CTAB (0.2 M, 50.0 ml) was mixed with 1.0 mM $NaAuCl_4$ (50.0 ml), $AgNO_3$ (0.1 M, 0.1 ml), and HCl (2.0 M, 0.1 ml). After gentle mixing of the solution, 78.8 mM ascorbic acid (0.7 ml) was added as a mild reducing agent. The color of the growth solution rapidly changed from dark yellow to colorless, indicating the formation of $AuCl_2^-$ ions. Finally, a portion of the seed solution (0.12 ml) was added to the growth solution. The solution gradually changed color to dark pink within 30 min, indicating the formation of GNR seeds. The as-prepared GNR seed solutions were used directly to prepare the differently shaped and sized Au core–Au–Ag shell NPs without any further purification.

2.3. Synthesis of differently shaped and sized Au core–Au–Ag shell NPs

The original pH value of the as-prepared GNR seed solution is pH 3.0. Twelve aliquots of the as-prepared GNR seed solutions (1.0 ml) were mixed separately with different volumes (0.08, 0.2, 0.4, and 0.8 ml) of 0.5 M glycine solutions to obtain the final pH values of 8.5, 9.5, and 10.5, respectively; note that the GNR seed solutions still contain silver and gold ions, as well as ascorbic acid. These mixtures were diluted with deionized water to give final volumes of 2.0 ml, and then they were incubated at room temperature without stirring for up to 6 h. The differently shaped and sized Au core–Au–Ag shell NPs were prepared simply by controlling the pH, glycine concentration, and incubation time.

2.4. Absorbance, transmission electron microscopy (TEM), and X-ray photoelectron spectra (XPS) measurements

A double-beam UV–vis spectrophotometer (Cintra 10e) obtained from GBC (Victoria, Australia) was used to measure the extinction of the prepared solutions. The TEM and high-resolution TEM (HR-TEM) images were recorded using H-7100 TEM (Hitachi, Tokyo, Japan) and Tena G2 HR-TEM (Fei, Amsterdam, The Netherlands) instruments, respectively. Energy-dispersive X-ray (EDX) spectra were recorded using the HR-TEM microscope. The XPS were measured by using an ESCALAB 250 (VG Scientific, UK) electron spectrometer. For TEM and XPS measurements, the as-prepared nanoparticles were subjected to four centrifuge-wash cycles to remove excess CTAB; centrifugation was conducted at 12,000 rpm for 15 min and deionized water (2.0 ml) was used for washing in each cycle. Prior to XPS analysis, the metal hydrosol was deposited on a silicon wafer (5×5 mm^2). It was performed using Al$K\alpha$ radiation and an analyzer pass energy of 20 eV without charge compensation. Au4f and Ag3d photoelectron spectra were measured at a detection angle of 90° with respect to the surface plane of the supporting substrate. For TEM measurements, the nanoparticles were deposited on a TEM grid coated with a thin layer of carbon. The dimensions of 100 Au core–Au–Ag shell NPs were measured for each sample to obtain the average size and the size distribution. The TEM measurements indicated that the Au core–Au–Ag shell NPs were monodisperse (>90%). The TEM images and UV–vis extinction coefficients measured from three different batches prepared under each set of conditions suggest that this synthetic method is highly reproducible.

2.5. Thermogravimetric analysis (TGA) measurements

The highly concentrated solution of Au core–Au–Ag shell NPs was purified by removing the excess CTAB and glycine through four centrifuge-wash cycles before being air dried and transferred to a platinum crucible for TGA measurements (Dynamic TGA 2950, New Castle, DE). In each cycle, centrifugation was conducted at 12,000 rpm for 15 min and deionized water (2.0 ml) was used for washing. After four centrifuge-wash cycles, most of the Au core–Au–Ag shell NPs precipitated in water, but were suspendable in an aqueous solution containing 5.0 μM CTAB and 2.0 μM glycine (pH 8.5). This finding suggests that most of the unbound CTAB and glycine were removed after being subjected to the four centrifuge/wash cycles. During the TGA experimental process, the temperature of the sample was raised from 25 to 800 °C at a rate of 10 °C/min.

2.6. Inductively coupled plasma-mass spectrometry (ICP-MS) measurements

The Au core–Au–Ag shell NPs prepared in different glycine solutions (0.02–0.2 M; pH 8.5–10.5) were subjected to four centrifuge-wash cycles to remove the excess CTAB as well as solutes that were physically adsorbed onto the surface of the as-prepared NPs; centrifugation was conducted at 12,000 rpm for 15 min and deionized water (2.0 ml) was used for washing in each cycle. The nanoparticles were then dissolved in 2.0% aqueous HNO_3 solution for ICP-MS measurements that were performed using an Elan 6000 ICP-MS instrument (Perkin–Elmer, Norwalk, CT). The concentrations of Au and Ag ions were estimated from the calibration curves of the standard solutions, which were used to estimate the total amounts of Au and Ag atoms in the Au core–Au–Ag shell NPs. The total amounts of Ag and Au atoms were then used to calculate the reduced fractions (%) of the Au and Ag ions.

2.7. Matrix-assisted laser desorption/ionization mass spectrometry (MALDI-MS) measurement

Mass spectrometry experiments were performed in the positive-ion mode of a time-of-flight mass spectrometer (Biflex III, Bruker, Germany) equipped with a 1.25-m flight tube. Desorption/ionization was effected by using a 337-nm nitrogen laser. The available accelerating voltages were within the range from 20 to −20 kV. Ten pulsed laser shots were applied under a laser power set at 43.5 μJ. Concentrated solutions (about 30-fold) of Au core–Au–Ag shell NPs, which had been undergone four centrifuge/wash cycles, were subjected to these MALDI-MS measurements.

2.8. Fourier transform infrared (FT-IR) spectroscopic measurement

GNR and Au core–Au–Ag shell NPs were subjected to four centrifuge-wash cycles. Portions of solutions containing glycine, CTAB, GNR, and Au core–Au–Ag shell NPs (the same samples that were used for the MALDI-MS measurements) were each deposited on a KBr pellet. After air drying, the FT-IR spectra of the four samples were recorded separately.

2.9. Zeta potential measurement

The Au core–Au–Ag shell NPs prepared in different glycine solutions (0.05–0.2 M; pH 9.7) were subjected to four centrifuge-wash cycles to remove the excess molecules that were physically adsorbed onto the surface of the as-prepared NPs; centrifugation was conducted at 12,000 rpm for 15 min and deionized water (2.0 ml) was used for washing in each cycle. Finally, the Au core–Au–Ag shell NPs were resuspended in 0.05 M glycine solutions (pH 9.7) for zeta potential measurements that were performed using a Malvern Zetasizer 3000 HS (Malvern Instruments Ltd., UK). The GNR seeds (pH 3.0) were subjected directly to zeta potential measurements.

3. Results and discussion

Fig. 1 presents the UV–vis spectra of the growth solutions in 0.02, 0.05, 0.1, and 0.2 M glycine solutions under alkaline conditions (pH 8.5, 9.5, and 10.5). The UV–vis extinction spectra all exhibit transverse (508–532 nm) and longitudinal (634–743 nm) SPR bands that are different from those for the GNR seeds, which are depicted by the dotted curve in Fig. 1. The ex-

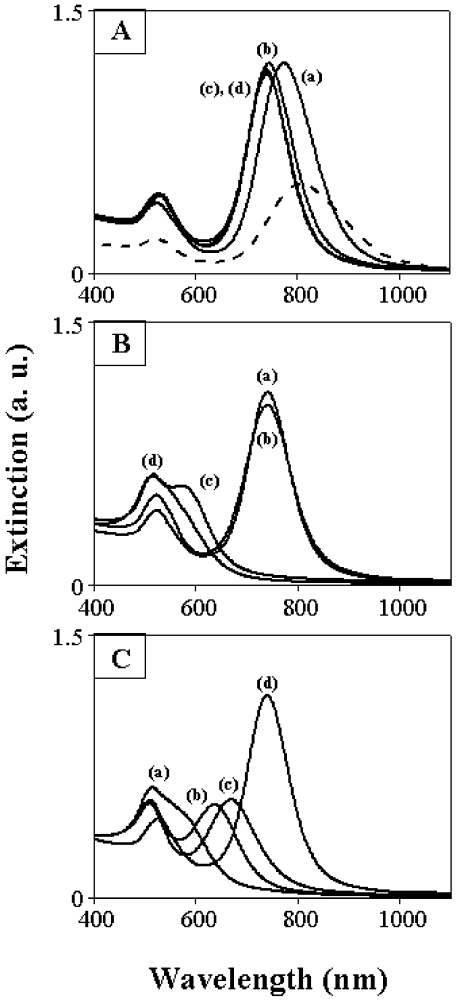

Fig. 1. UV–vis extinction spectra for the original GNRs and Au core–Au–Ag shell NPs prepared in (a) 0.02, (b) 0.05, (c) 0.1, and (d) 0.2 M glycine solutions containing 0.19 mM gold ions, 0.049 mM silver ions, and 0.27 mM ascorbic acid at (A) pH 8.5, (B) pH 9.5, and (C) pH 10.5. The dotted curve in (A) stands for the original GNR seeds. Prior to measuring the extinction, all samples were diluted twofold using deionized water.

tinctions for the transverse and longitudinal SPR bands of the growth solutions are both greater than those of the GNR seed solution. It is known that changes in the dielectric function and the aspect ratio, as well as the deposition of Ag onto the surface of GNRs, influence the spectral properties of GNRs [31]. To test the effect that changing the dielectric constant of the glycine solutions has on the GNRs, we resuspended the NPs (prepared in 0.02 M glycine at pH 9.5) in various glycine solutions (0.02–0.2 M; pH 8.5–10.5). We did not observe any significant changes in the UV–vis spectra, which rules out the dielectric function playing any role in determining the optical properties. Generally, blue shifts of the longitudinal SPR band indicate that depositions of silver and gold on the surface of GNRs and changes in the aspect ratio of the GNRs have occurred [30]. In addition, the changes in the morphologies of the NRs are taken into account for the differential UV–vis spectra. We point out that the formation of Au–Ag nanocomposites is the primary reason for the increases in intensity of the longitudinal SPR band.

In our previous study, TEM images and EDX data confirmed the formation of Au core–Au–Ag shell NPs from GNRs using a similar condition [30]. The TEM images displayed in Fig. 2 provide direct evidence for the formation of the different Au core–Au–Ag shell NPs. The XPS (Fig. 3) show the distribution of both Au and Ag in the surface (with the penetration depth less than 2 nm), which supports the Au–Ag alloy structure in the shell. High qualities of the Au core–Au–Ag shell NPs support our reasoning that the formation of Au–Ag nanocomposites is the primary reason for the increases in intensity of the longitudinal SPR band. Table 1 summarizes the physical properties of the as-prepared Au core–Au–Ag shell NPs, such as their sizes, shapes, and SPR extinctions; the descriptors L_1, D_1, and D_2 are defined in Scheme 1. The TEM images confirm that only slight changes occur in the morphologies of the Au–Ag NRs prepared at pH 8.5 in the different glycine solutions. Although the GNRs incubated in 0.02 and 0.05 M glycine solutions at pH 9.5 have similar extinction spectra, the TEM images reveal that they have primarily rod-shaped structures in the former case, but mostly dumbbell-shaped structures in the latter. Under the same conditions, mostly gold nanoparticles and silver nanoparticles formed in the absence of gold seeds. In order to estimate the amounts of Au and Ag atoms in the Au core–Au–Ag shell NPs, we dissolved the NPs in 2% HNO_3 prior to ICP-MS measurements. The ICP-MS measurements also reveal a difference between these structures: their molar ratios of Ag^{107}/Au^{197} are 0.13 and 0.17, respectively. The fact that increases in the molar ratio of Ag^{107}/Au^{197} upon increasing glycine concentration was supported by the EDX data as displayed in Fig. 4. We conducted UV–vis spectroscopic extinction measurements to determine whether the thus-prepared Au core–Au–Ag shell NPs would dissolve in aqueous HNO_3 solution. The disappearance of the transverse and longitudinal SPR bands and the appearance of a band at 305 nm (Au(I) ions) indicate that the Au core–Au–Ag shell NPs did indeed dissolve in 2% HNO_3. Taking the results from the UV–vis spectroscopic extinction, TEM, and ICP-MS measurements together, we conclude that the Au core–Au–Ag shell NPs formation was successful.

Our ICP-MS measurements indicate that the reduced fractions of Au^{197} and Ag^{107} decreased from 95 to 74% and from 94 to 66%, respectively, upon increasing the glycine concentration from 0.05 to 0.2 M at pH 10.5. The TEM images display different morphologies for the Au core–Au–Ag shell NPs that were prepared in 0.1 and 0.2 M glycine solutions (pH 9.5); they have aspect ratios of 2.3 and 2.0, respectively. The decrease in the aspect ratio agrees with the dramatic changes observed in the UV–vis extinction spectra (Fig. 1B). Because of increases in the width of the NRs and the formation of dumbbell- and peanut-shaped NPs, we suggested that Au and Ag atoms were deposited at the {110} facets (two sides) as well as {111} facets of NRs as displayed in Fig. 5A [25,30]. The HRTEM images displayed in Fig. 5B show the crystalline structures of NPs. The TEM images (Figs. 2B and 2C) also indicate that the greatest number of spherically shaped Au core–Au–Ag shell NPs were prepared in the 0.2 M glycine solution at pH 9.5 and in the 0.02 M glycine solution at pH 10.5. We believe that the twinned particles that are highlighted by the arrowhead in the

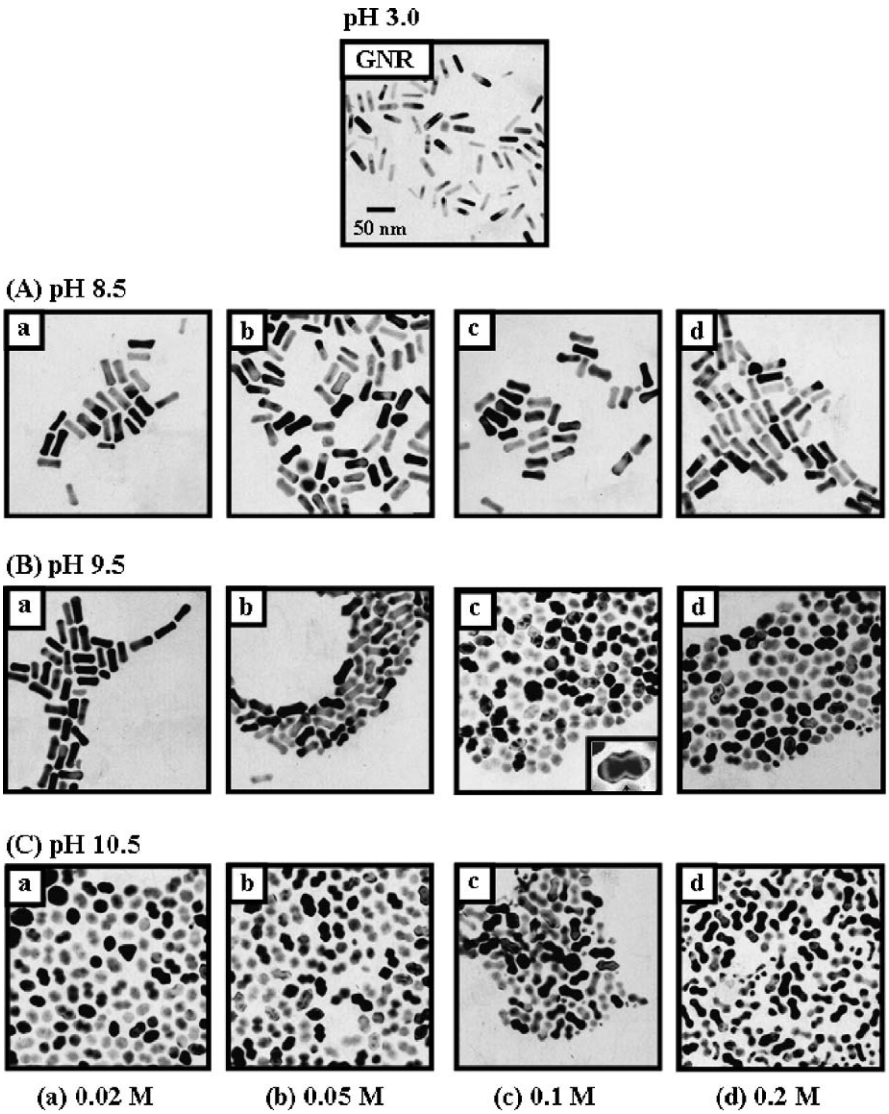

Fig. 2. TEM images of the original GNR seeds and the Au core–Au–Ag shell NPs obtained at different values of pH—(A) pH 8.5, (B) pH 9.5, and (C) pH 10.5—and in glycine solutions having different concentrations: (a) 0.02, (b) 0.05, (c) 0.1, and (d) 0.2 M. Scale bar: 50 nm. Other conditions are identical to those described in Fig. 1.

magnified TEM image (inset) in Fig. 2B(c) are precursors of the spherically shaped NPs in Figs. 2B(d) and 2C(a). During the growth process, the changes in the shapes of the NPs are due to depositions of Au and Ag atoms on the surface. At pH 10.5, the spherically shaped Au–Ag NPs are dominant in low-concentration (<0.05 M) glycine solutions. This situation exists because the fraction of CTAB cations decreases while that of glycine anions increases upon increasing the value of pH and probably destruct the well-organized CTAB bilayer along the {110} facets. At pH 10.5, the transformation from peanut-like to dumbbell-like shapes in the TEM images (Fig. 2C) occurs when the glycine concentration was increased from 0.05 to 0.2 M. We note that the absolute amount of Au in the Au core–Au–Ag shell NPs is higher in 0.05 M glycine as a result of the greater oxidizing ability of gold ions at low glycine concentrations; (less) fractions of gold ions exist in the form of gold–glycine complexes. The changes in both the morphology and the deposition of silver and gold atoms explain the red shift of the longitudinal extinction bands in the UV–vis extinction spectra (Fig. 1C).

At the same value of pH, we prepared differently sized and shaped Au core–Au–Ag shell NPs in the presence of various concentrations of glycine, which indicates that glycine ($pK_{a2} = 9.7$) was involved in the synthesis of the Au core–Au–Ag shell NPs. The formation of differently sized and shaped Au core–Au–Ag shell NPs suggests that, in addition to the concentrations of ascorbic acid, $NaAuCl_4$, and $AgNO_3$ and the pH, glycine plays a role in determining the sizes and shapes of the Au–Ag NPs. The TEM images (Fig. 2) reveal that the effect that the glycine concentration has on the synthesis of Au–Ag NPs is small at pH 8.5 relative to those that occur at pH 9.5 and 10.5. Because of increases in both the pH and the glycine concentration, the total number of positively charged species on the GNR surface decreases; the zeta potentials were 78.9 and 38.4 mV for the CTAB-capped GNR seeds (pH 3.0) and the Au core–Au–Ag shell NPs prepared in 0.05 M glycine (pH 9.7), re-

spectively. This finding suggests that changes in the amount of electronic charge on the GNR surfaces probably play a role in determining their morphology [33]. The role that glycine plays during the synthesis of the Au core–Au–Ag shell NPs might be affected by three different factors: (1) Upon increasing the value of pH, glycine molecules carry a greater amount of negative charge, which allows them to form stronger complexes with gold and silver ions [34]. The formation constant for the complex of silver–glycine (ML_2) is $\log K_f = 6.92$ [35]. We point out that we did not observe AgBr precipitation in the glycine buffers as that in the absence of glycine. As a result, the oxidizing abilities of gold and silver ions decrease as the glycine concentration increases. (2) The morphology of the CTAB micelles might be different in the presence of large amounts of

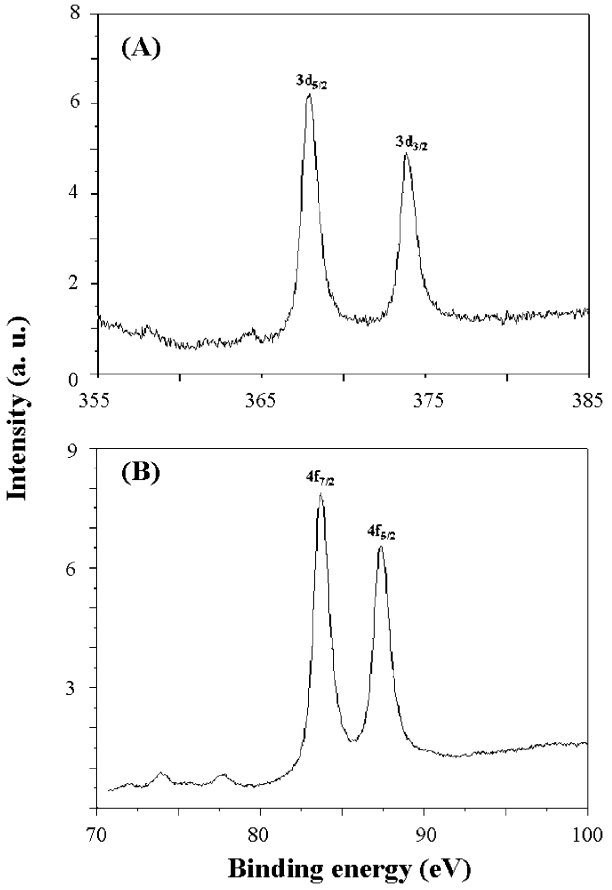

Fig. 3. XPS spectra of (A) Ag3*d* and (B) Au4*f* in the Au core–Au–Ag shell NPs.

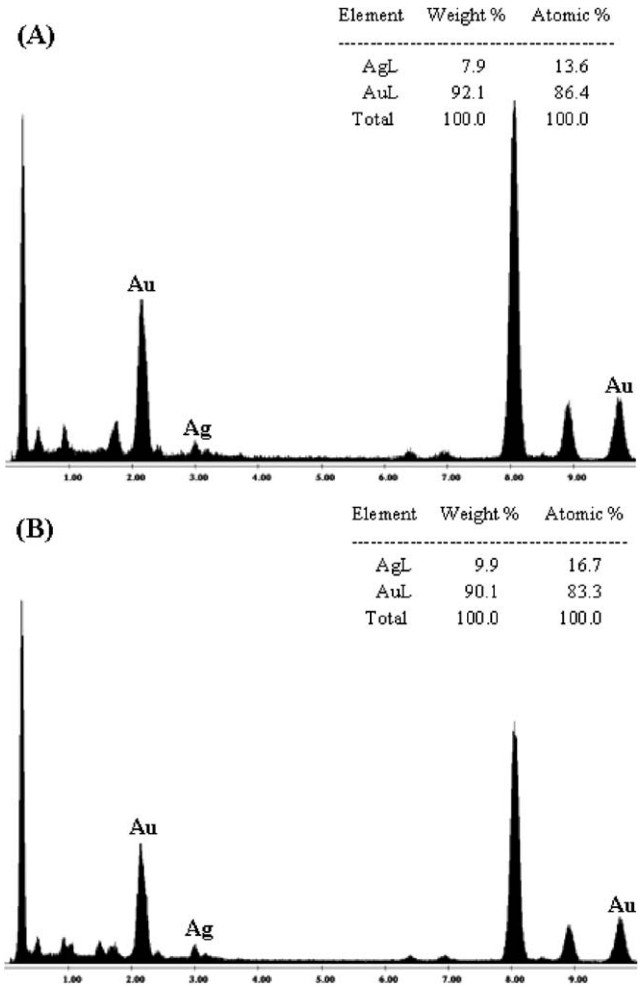

Fig. 4. EDX analysis of the Au core–Au–Ag shell NPs obtained at pH 9.5 and in glycine solutions having different concentrations: (A) 0.02 M and (B) 0.05 M. Other conditions are identical to those described in Fig. 1.

Table 1
The physical and optical properties of the GNRs and the Au core–Au–Ag shell NPs[a]

	GNR	pH 8.5				pH 9.5				pH 10.5			
		0.02 M	0.05 M	0.1 M	0.2 M	0.02 M	0.05 M	0.1 M	0.2 M	0.02 M	0.05 M	0.1 M	0.2 M
L_1 (nm)	40 ± 3	49 ± 3	47 ± 3	50 ± 3	50 ± 2	49 ± 4	48 ± 3	44 ± 3	44 ± 3	44 ± 3	43 ± 4	44 ± 4	49 ± 3
D_1 (nm)	11 ± 1	15 ± 2	15 ± 2	16 ± 2	16 ± 2	14 ± 1	14 ± 2	20 ± 3	22 ± 2	19 ± 2	17 ± 2	16 ± 2	15 ± 2
D_2 (nm)	–	20 ± 2	21 ± 2	22 ± 3	20 ± 1	19 ± 2	23 ± 2	26 ± 3	25 ± 2	25 ± 2	24 ± 2	22 ± 2	22 ± 2
L_1/D_1	3.6	3.3	3.1	3.1	3.2	3.5	3.4	2.3	2.0	2.3	2.5	2.8	3.3
Au (%)[b]	27	70	82	99	96	96	94	100	96	96	95	96	74
Ag (%)[b]	0	45	47	46	54	59	78	93	87	92	94	86	66
Shape[c]	Rod	Rod	Rod	Rod	Rod	Rod	Dumbbell	Peanut	Peanut	Peanut	Peanut	Peanut	Peanut
λ_T (nm)	518	523	528	532	525	521	521	515	513	513	508	508	525
λ_L (nm)	807	772	743	740	738	740	740	573	–	570	634	667	738

[a] The descriptors L_1, D_1, and D_2 are defined in Scheme 1. The descriptors λ_T and λ_L represent the maximum wavelengths of the transverse and longitudinal SPR extinctions, respectively.

[b] The reduced fraction (%) is estimated from the ICP-MS data.

[c] The shapes are described as the main component of the as-prepared NPs under different conditions.

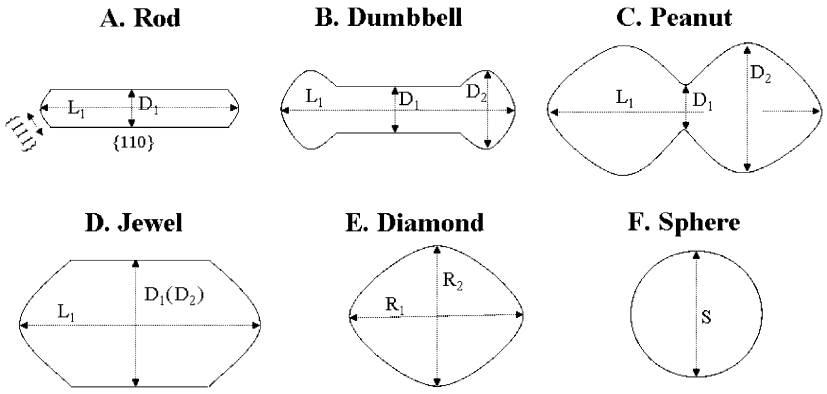

Scheme 1. Morphologies of the Au core–Au–Ag shell NPs prepared under the different conditions.

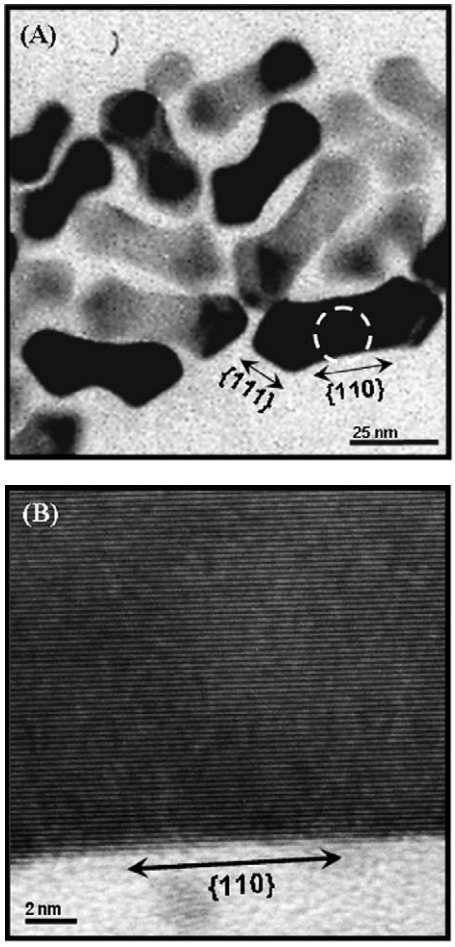

Fig. 5. TEM and HRTEM of representative Au core–Au–Ag shell NPs.

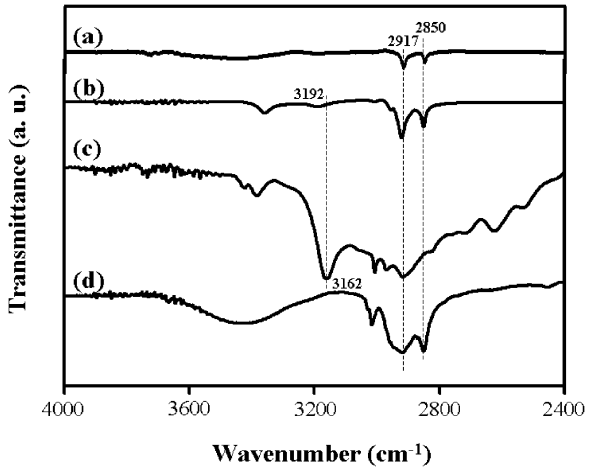

Fig. 6. FT-IR spectra of (a) CTAB-modified GNRs, (b) CTAB and glycine-modified Au core–Au–Ag shell NPs prepared in 0.2 M glycine solution at pH 9.7, (c) glycine, and (d) CTAB. The peaks at 2850 and 2917 cm^{-1} reflect the symmetric and asymmetric C–H stretching vibrations, respectively. The vibration at 3162 cm^{-1} reflects the asymmetric stretching vibration of the NH_3^+ unit.

anionic glycine, leading to the formation of various sizes and shapes of Au–Ag NPs. (3) At high concentrations of glycine, a greater number of glycine molecules exist on the surface of the Au–Ag NPs, as evidenced by the FT-IR spectra presented in Fig. 6 (curves b and c). The band at 3162 cm^{-1}, which corresponds to the asymmetric stretching vibration of the NH_3^+ units of glycine molecules, shifts to 3192 cm^{-1} in the presence of the Au core–Au–Ag shell NPs. The bands at 2850 (hidden in a broad band in the case of glycine) and 2917 cm^{-1} (curves c and d), which we assign to the symmetric and asymmetric C–H vibration of glycine and CTAB molecules, appear in the spectrum of the dry Au core–Au–Ag shell NPs (curve b) [36]. When comparing the IR spectra in Figs. 6a, 6b, and 6d, we conclude that CTAB molecules were bound to the Au core–Au–Ag shell NPs. We point out that there are no peaks corresponding to glycine and CTAB in the IR spectrum for the supernatant after four centrifugation-washing cycles. These observations reveal that glycine and CTAB molecules are both adsorbed on the Au core–Au–Ag shell NPs. The adsorption of glycine molecules on the nanostructure is also supported by the detection of glycine at m/z 75.949 $[M + H]^+$ (mass spectrum not shown); we did not observe such a peak for the Au–Ag NPs and the GNR seeds that we prepared in the absence of glycine.

TGA measurements further confirmed the adsorption of glycine and CTAB molecules (Fig. 7). Curves a and b in Fig. 7A display weight losses of 100 and 92% at 259 °C for pure CTAB powder and CTAB adsorbed on the GNR seeds, respectively. Desorption curve c is significantly different from curves a and b, which suggests that other molecules are adsorbed on the Au core–Au–Ag shell NPs. We note that the weight loss is ca. 38% in the region from 190 to 230 °C in curve c, which cor-

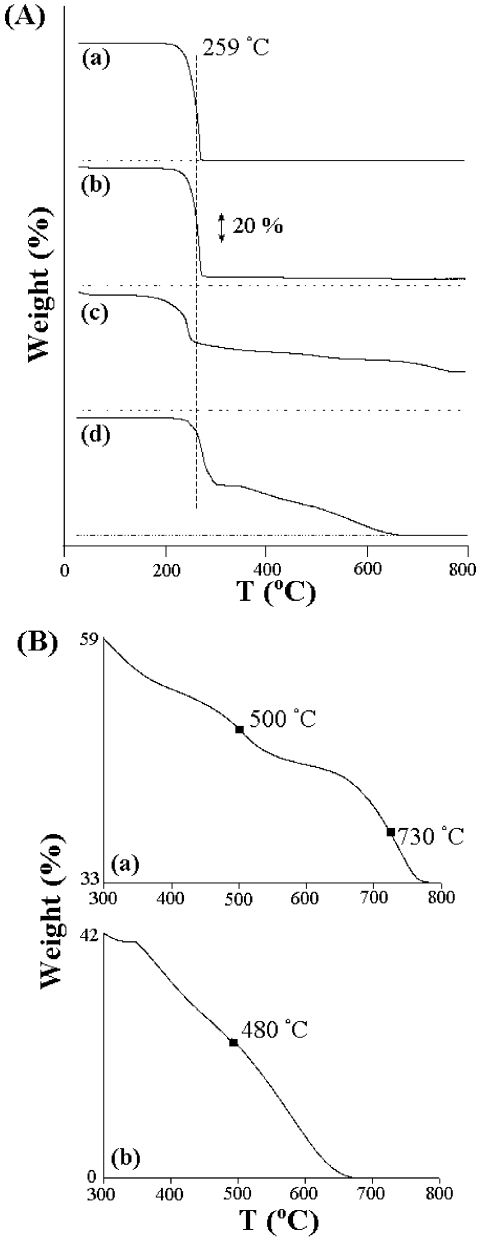

Fig. 7. (A) TGA data recorded for pure CTAB (curve a), CTAB-modified GNRs (curve b), CTAB-and-glycine-modified Au core–Au–Ag shell NPs prepared in 0.2 M glycine solution at pH 9.7 (curve c), and pure glycine (curve d). (B) Curves c and d in (A) replotted to present their differences more clearly.

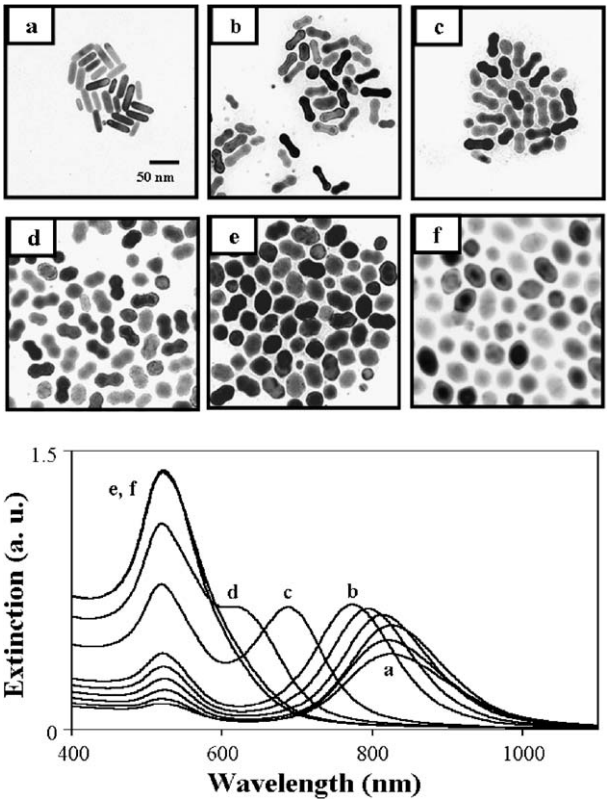

Fig. 8. TEM images and UV–vis extinction spectra displaying the evolution of the formation of Au core–Au–Ag shell NPs incubated in 0.1 M glycine solution at pH 9.7 as a function of time. (a) 0, (b) 5, (c) 10, (d) 20, (e) 30, and (f) 60 min. Other conditions are identical to those described in Fig. 1.

responds to the desorption of a mixture of CTAB and glycine; the other two weight losses occurred in the ranges 400–600 °C (14%) and 600–770 °C (12%). When compared with that for pure glycine (curve d), we can confirm that glycine was adsorbed on the Au core–Au–Ag shell NPs. Curves a and b in Fig. 7B display clear differences. The desorption temperature for glycine molecules is higher in the Au core–Au–Ag shell NPs than it is in pure glycine, which further supports the notion of the adsorption of glycine molecules on the Au core–Au–Ag shell NPs. Moreover, the weight losses in the ranges 400–600 and 600–770 °C both increased upon increasing the glycine concentration. For example, the losses in the range 400–600 °C were 2.5 and 14%, respectively, in solutions containing 0.05 and 0.2 M glycine (pH 9.7), while they were 2.3 and 12% between 600 and 770 °C.

The UV–vis extinction spectra (Fig. 1) and the TEM images (Fig. 2) also indicate the formation of different Au core–Au–Ag shell NPs at the same glycine concentration but different values of pH. The fraction of monoanionic ascorbate species, which are capable of reducing gold and silver ions, increases as the value of pH increases (the values of pK_{a1} and pK_{a2} for ascorbic acid are 4.10 and 11.79, respectively) [30,32,37]. As a result, the amount of deposited silver and the reaction rate both increase upon increasing the pH. Our hypothesis is supported by the results of ICP-MS measurements, which indicate that the molar ratio of Ag^{107}/Au^{197} increases from 0.09 to 0.18 as the value of pH varies from 8.5 to 10.5 in 0.1 M glycine solution.

To further investigate the formation of the different morphologies of the Au core–Au–Ag shell NPs, we subjected the Au core–Au–Ag shell NPs prepared in 0.1 M glycine (pH 9.7) after different periods of time to UV–vis spectroscopic extinction, ICP-MS, and TEM measurements. Note that we terminated the reactions by adding small amounts of concentrated HCl to bring the pH of the mixtures to a value of 3.0. This method is effective for stopping the reaction, as evidenced by the fact that no changes occurred in the UV spectra within 3 h. Fig. 8 displays the TEM images and UV–vis extinction spectra of the Au core–Au–Ag shell NPs prepared over periods of time from 0 to 60 min. No additional NPs were observed in

Table 2
The shapes and physical properties of the GNRs and the Au core–Au–Ag shell NPs[a]

Time (min)	Shape	L_1 (nm)	D_1 (nm)	D_2 (nm)	L_1/D_1	R_1 (nm)	R_2 (nm)	S (nm)	Yield (%)	Au (%)[b]	Ag (%)[b]
0	Rod	40 ± 3	11 ± 1	N[c]	3.6	N	N	N	90	30	11
5	Dumbbell	44 ± 3	13 ± 1	17 ± 1	3.5	N	N	N	100	55	33
10	Dumbbell	46 ± 3	15 ± 1	20 ± 1	3.1	N	N	N	100	79	57
20	Peanut	46 ± 3	18 ± 1	25 ± 1	2.5	N	N	N	47	95	93
	Jewel	40 ± 3	24 ± 1	24 ± 1	1.7	N	N	N	27		
	Diamond	N	N	N	N	32 ± 1	29 ± 1	N	16		
	Sphere	N	N	N	N	N	N	27 ± 2	10		
30	Peanut	48 ± 3	24 ± 2	29 ± 1	2.0	N	N	N	25	96	95
	Jewel	45 ± 3	28 ± 2	28 ± 2	1.6	N	N	N	35		
	Diamond	N	N	N	N	34 ± 3	30 ± 2	N	20		
	Sphere	N	N	N	N	N	N	27 ± 2	20		
60	Jewel	44 ± 3	28 ± 2	28 ± 2	1.6	N	N	N	28	91	90
	Diamond	N	N	N	N	31 ± 2	28 ± 2	N	23		
	Sphere	N	N	N	N	N	N	25 ± 2	49		

[a] The descriptors L_1, D_1, D_2, R_1, R_2, and S are defined in Scheme 1.
[b] The reduced fraction (%) is estimated from the ICP-MS data.
[c] N: Not observed.

the TEM images during the evolution of the formation of Au core–Au–Ag shell NPs, which support our reasoning that the formation of Au core–Au–Ag shell NPs is the primary reason for increases in the longitudinal SPR extinction band. The TEM images and the increases in the amounts of gold and silver (Table 2) clearly indicate that the deposition of Au and Ag atoms begins at the two ends. These results support the formation of Au core–Au–Ag shell. After ca. 20 min, the peanut-shaped and dumbbell-shaped NPs disappeared and the spherically shaped Au core–Au–Ag shell NPs formed. When the stress/strain ratio is too high, the peanut-shaped and dumbbell-shaped Au core–Au–Ag shell NPs break to form spherically shaped (with diameter 25 ± 2 nm) and diamond-shaped ($R_1 = 31 \pm 2$ nm; $R_2 = 28 \pm 2$ nm) particles; this situation is supported by the disappearance of the peanut-shaped Au core–Au–Ag shell NPs and an increase in the number of spherical particles within the time period from 30 to 60 min. After reacting for 60 min, the jewel-, diamond-, and sphere-shaped Au core–Au–Ag shell NPs have abundances of ca. 28, 23, and 49%, respectively. The values of L_1 and D_1 for the jewel-shaped Au core–Au–Ag shell NPs are 44 ± 3 and 28 ± 2 nm, respectively; these values indicate that the deposition of Au and Ag atoms has occurred on the peanut- and dumbbell-shaped Au core–Au–Ag shell NPs (see Table 2). On the basis of these results, we suggest that the formation of the Au core–Au–Ag shell NPs is determined by a balance between the concentration buildup (gold and silver ions) and the competition between the ligands and stabilizing molecules (CTAB and glycine) for the particle's surface [38,39]. Our results also indicate that differently shaped Au core–Au–Ag shell NPs can be prepared by controlling the reaction time.

4. Conclusions

In this paper, we demonstrate that controlling the pH and glycine concentration can allow the preparation of dumbbell- and peanut-shaped Au core–Au–Ag shell NPs in high yields. We have also deduced the roles that glycine plays in the synthesis of the Au core–Au–Ag shell NPs, which include minimize the formation of AgCl, AgBr, and Ag_2O precipitates, retarding the deposition of Au^0 and Ag^0 onto the surface of the GNR seeds by reducing the oxidizing ability of the gold and silver ions, and stabilizing the NPs. The changes that occur in the shapes of the Au–Ag NPs as a function of time (0–60 min), reveal that the reaction time is another factor that can be used to control the morphologies of the Au core–Au–Ag shell NPs.

Acknowledgments

This work was supported by the National Science Council of Taiwan under contracts NSC-94-2113-M-002-008, NSC-94-2113-M-002-036, and NSC94-2515-S-002-009.

References

[1] J. Hu, T.W. Odom, C.M. Lieber, Acc. Chem. Res. 32 (1999) 435.
[2] M.A. El-Sayed, Acc. Chem. Res. 34 (2001) 257.
[3] M.H. Huang, S. Mao, H. Feick, H. Yan, Y. Wu, H. Kind, E. Weber, R. Russo, P. Yang, Science 292 (2001) 1897.
[4] W.U. Huynh, J.J. Dittmer, A.P. Alivisatos, Science 295 (2002) 2425.
[5] K. Elteto, X.-M. Lin, H.M. Jaeger, Phys. Rev. B 71 (2005) 2054121.
[6] O. Wilson, G.J. Wilson, P. Mulvaney, Adv. Mater. 14 (2002) 1000.
[7] F. Favier, E.C. Walter, M.P. Zach, T. Benter, R.M. Penner, Science 293 (2001) 2227.
[8] D.H. Wang, R. Kou, M.P. Gil, H.P. Jakobson, J. Tang, D.H. Yu, Y.F. Lu, J. Nanosci. Nanotech. 5 (2005) 1904.
[9] Y. Sun, Y. Xia, Analyst 128 (2003) 686.
[10] C. Sönnichsen, T. Franzl, T. Wilk, G. von Plessen, J. Feldmann, O. Wilson, P. Mulvaney, Phys. Rev. Lett. 88 (2002) 077402.
[11] C.J. Orendorff, S.C. Baxter, E.C. Goldsmith, C.J. Murphy, Nanotechnology 16 (2005) 2601.
[12] S. Link, M.A. El-Sayed, J. Phys. Chem. B 103 (1999) 8410.
[13] A.D. McFarland, R.P. Van Duyne, Nano Lett. 3 (2003) 1057.
[14] S.-J. Park, S. Kim, S. Lee, Z.G. Khim, K. Char, T. Hyeon, J. Am. Chem. Soc. 122 (2000) 8581.
[15] F. Kim, J.H. Song, P. Yang, J. Am. Chem. Soc. 124 (2002) 14316.
[16] Z. Liu, Z. Hu, J. Liang, S. Li, Y. Yang, S. Peng, Y. Qian, Langmuir 20 (2004) 214.

[17] P. Zhang, L. Gao, Langmuir 19 (2003) 208.
[18] B.R. Martin, D.J. Dermody, B.D. Reiss, M. Fang, L.A. Lyon, M.J. Natan, T.E. Mallouk, Adv. Mater. 11 (1999) 1021.
[19] B.M.I. van der Zande, M.R. Böhmer, L.G.J. Fokkink, C. Schönenberger, Langmuir 16 (2000) 451.
[20] V.M. Cepak, C.R. Martin, J. Phys. Chem. B 102 (1998) 9985.
[21] T. Thurn-Albrecht, J. Schotter, G.A. Kästle, N. Emley, T. Shibauchi, L. Krusin-Elbaum, K. Guarini, C.T. Black, M.T. Tuominen, T.P. Russel, Science 290 (2000) 2126.
[22] Y.-Y. Yu, S.-S. Chang, C.-L. Lee, C.R.C. Wang, J. Phys. Chem. B 101 (1997) 6661.
[23] K. Esumi, K. Matsuhisa, K. Torigoe, Langmuir 11 (1995) 3285.
[24] N.R. Jana, L. Gearheart, C.J. Murphy, J. Phys. Chem. B 105 (2001) 4065.
[25] B. Nikoobakht, M.A. El-Sayed, Chem. Mater. 15 (2003) 1957.
[26] N.R. Jana, L. Gearheart, C.J. Murphy, Chem. Commun. (2001) 617.
[27] C.J. Johnson, E. Dujardin, S.A. Davis, C.J. Murphy, S. Mann, J. Mater. Chem. 12 (2002) 1765.
[28] J. Gao, C.M. Bender, C.J. Murphy, Langmuir 19 (2003) 9065.
[29] N.R. Jana, L. Gearheart, C.J. Murphy, Adv. Mater. 13 (2001) 1389.
[30] C.-C. Huang, Z. Yang, H.-T. Chang, Langmuir 20 (2004) 6089.
[31] C.S. Ah, S.D. Hong, D.-J. Jang, J. Phys. Chem. B 105 (2001) 7871.
[32] M. Liu, P. Guyot-Sionnest, J. Phys. Chem. B 108 (2004) 5882.
[33] J. Pérez-Juste, L.M. Liz-Marzán, S. Carnie, D.Y.C. Chan, P. Mulvaney, Adv. Funct. Mater. 14 (2004) 571.
[34] T. Shoeib, K.W.M. Siu, A.C. Hopkinson, J. Phys. Chem. A 106 (2002) 6121.
[35] F.M.M. Morel, Principles of Aquatic Chemistry, Wiley–Interscience, New York, 1983, p. 237.
[36] B. Nikoobakht, M.A. El-Sayed, Langmuir 17 (2001) 6368.
[37] T. Pal, S. De, N.R. Jana, N. Pradhan, R. Mandal, A. Pal, A.E. Beezer, J.C. Mitchell, Langmuir 14 (1998) 4724.
[38] S. Chen, Z.L. Wang, J. Ballato, S.H. Foulger, D.L. Carroll, J. Am. Chem. Soc. 125 (2003) 16,186.
[39] T.K. Sau, C.J. Murphy, J. Am. Chem. Soc. 126 (2004) 8648.